Journal of Environmental Science 12 (2025) 01-15

IES University of Rajshahi

Journal of Environmental Science
https://jenvos ci.com

ANALYZING DECADAL MANGROVE COVER CHANGE IN THE BANGLADESHI SUNDARBANS USING REMOTE SENSING

Md. Imran Hossain*1, Sabbir Ahmed Sweet2, Nafia Muntakim1, Mst. Tasnima Khatun1, Shanita Tahnin2, Tomalika Biswas3, Md. Mujibor Rahman4, Md. Redwanur Rahman1

1 Institute of Environmental Science, University of Rajshahi, Rajshahi, Bangladesh,
2 Department of Geography and Environmental Studies, University of Rajshahi, Rajshahi, Bangladesh,
3 Department of Geosciences, Colorado State University, USA,
4 Environmental Science Discipline, Khulna University, Khulna, Bangladesh

ARTICLE INFO

Keywords:
Ecosystem monitoring, Land Cover Classification, Mangrove Degradation, Remote Sensing, Sundarbans

ABSTRACT

The Sundarbans Mangrove Forest in Bangladesh, the world's largest tidal mangrove ecosystem, has undergone substantial ecological change over the past five decades. This study investigates land cover transformation from 1975 to 2025 using atmospherically corrected Landsat imagery and supervised Maximum Likelihood Classification (MLC). The landscape was categorized into four classes-Dense Forest, Sparse Forest, Bare Soil, and Water-across six periods to identify long-term spatial patterns and ecological vulnerabilities. Results reveal a 31.07% reduction in Dense Forest area (from 3914.06 km² to 2697.82 km²), accompanied by a 383.67% increase in Sparse Forest and a nearly 300% rise in Bare Soil. These trends reflect forest fragmentation, degradation, and progressive thinning of canopy cover, largely driven by upstream hydrological alterations, salinity intrusion, and increasing anthropogenic pressure. While the Water class showed minimal net change in surface extent, localized gains and losses aligned with tidal influence and sedimentation cycles. Transition matrices and gain-loss analyses identified southern estuarine margins and forest edges as degradation hotspots, while northern zones exhibited localized signs of regeneration. The classification results achieved high accuracy levels (84% to 92.3%) with Kappa values exceeding 0.80, confirming methodological reliability. This study emphasizes the need for integrated conservation, restoration planning, and improved freshwater governance to mitigate further degradation. The findings provide a scientific basis for adaptive ecosystem management in one of the world's most climate-sensitive coastal environments.

1. Introduction

The Sundarbans Mangrove Forest, located at the confluence of the Ganges, Brahmaputra, and Meghna rivers, is the largest continuous mangrove forest in the world, stretching across approximately 10,000 square kilometers in Bangladesh and India (Giri *et al.,* 2011). This unique ecosystem plays an essential role in biodiversity conservation, carbon sequestration, storm protection, and supporting the livelihoods of millions of people. The Sundarbans provide critical habitat for iconic and endangered species including the Royal Bengal Tiger (*Panthera tigris tigris*), estuarine crocodiles

Corresponding author.
E-mail address: imransizar786@gamil.com (Md. Imran Hossain)
Receive 24 April 2025; Revised Received 17 June 2025; Accepted 26 June 2025;
Available Online 21 December 2025;
Published by Institute of Environmental Science, University of Rajshahi.

(*Crocodylus porosus*), and the Irrawaddy dolphin (*Orcaella brevirostris*) (Uddin *et al.,* 2014; Ghosh *et al.,* 2016).

Despite its ecological and socio-economic importance, the Sundarbans are facing unprecedented degradation due to both anthropogenic and climatic stressors. Population pressure, illegal logging, shrimp farming, and infrastructural development continue to encroach on mangrove habitats. Simultaneously, climate change-induced factors such as sea-level rise, salinity intrusion, increased frequency of cyclones, and coastal erosion further exacerbate the forest's vulnerability (Dasgupta *et al.,* 2015; Patra, 2024). In particular, altered river discharge caused by upstream water management practices, including the Farakka Barrage, has reduced the availability of freshwater, enhanced salinization, and shifted vegetation composition (Uddin *et al.,* 2014; Bomer *et al.,* 2020). Similar patterns of reduced freshwater flow and increasing salinity stress have also been identified in recent studies analyzing decadal mangrove change, highlighting regional-scale hydrological and anthropogenic impacts (Emch & Peterson, 2006; Chowdhury & Hafsa, 2022; Kanjin *et al.,* 2024). However, while previous studies have advanced understanding of vegetation health and spectral variability, they have not fully explored multi-decadal, statistically grounded land cover classification across ecologically distinct categories.

Given these dynamics, there is an urgent need for regular, long-term monitoring of land cover dynamics in the Sundarbans to inform conservation and policy efforts (Bhattacharjee *et al.,* 2021; Kundu *et al.,* 2020). Remote sensing has emerged as an indispensable tool for such monitoring due to its ability to provide synoptic, repeatable observations across large and inaccessible landscapes (Kuenzer *et al.,* 2011; Negassa *et al.,* 2020). Among various remote sensing techniques, supervised classification methods like the Maximum Likelihood Classification (MLC) have proven effective for producing reliable land cover maps, particularly in heterogeneous and fragmented ecosystems like mangrove forests (Al-doski *et al.,* 2013; Jensen, 2015).

While studies using vegetation indices such as the Normalized Difference Vegetation Index (NDVI) have been helpful in tracking vegetation health (Bhattacharjee *et al.,* 2021), they do not provide explicit land cover category delineations. NDVI is limited to spectral indicators of greenness and cannot differentiate between ecologically significant classes like sparse vs. dense forest or soil vs. degraded vegetation (Tucker, 1979; Huete *et al.,* 2002). In contrast, MLC facilitates a more detailed and accurate classification of multiple land cover types by assigning pixels based on statistical probabilities and training samples.

Despite the potential of MLC for mapping complex vegetation structures, relatively few studies have conducted multi-decadal classification of the Sundarbans using this method. MLC offers a statistically robust approach especially suited for ecosystems with overlapping spectral characteristics like mangrove forests, making it a suitable choice for this long-term analysis. One of the earlier efforts to examine Sundarbans mangrove cover change using Landsat imagery applied multiple classification methods including MLC, NDVI differencing, and subpixel classification to assess forest dynamics between 1989 and 2000 (Emch & Peterson, 2006). Existing literature either focuses on short time spans or lacks robust accuracy assessments and spatial change detection (Sunkur *et al.,* 2024). Furthermore, little emphasis has been placed on identifying transition hotspots - areas where rapid or frequent class change occurs - which are crucial for prioritizing restoration or protective interventions (Roy *et al.,* 2025).

This study seeks to bridge these gaps by conducting a comprehensive, multi-decadal land cover classification and transformation analysis of the Sundarbans from 1975 to 2025. Using atmospherically corrected Landsat data and supervised MLC, we categorized the landscape into four classes: Water, Bare Soil, Sparse Forest, and Dense Forest. We also performed spatiotemporal analyses to map transition hotspots and assess ecological vulnerability. This approach complements and extends previous efforts such as Kanjin *et al.* (2024), who used NDVI and PCA to detect mangrove degradation patterns over three decades, though their classification lacked categorical delineation between forest conditions.

The specific objectives of this research are to: Conduct a long-term, quantitative analysis of land cover changes from 1975 to 2025 in the Sundarbans Mangrove Forest using supervised Maximum Likelihood Classification (MLC). Quantify major land cover transitions and identify ecological degradation zones in the Sundarbans between 1975 and 2025. Provide long-term, evidence-based insights for conservation and restoration planning.

2. Materials and Methods

2.1 Study Area

In this study, the Bangladeshi part of the Sundarbans has been selected as the primary focus area (Fig. 1). It lies between 21.5° to 22.5° N latitude and 88.0° to 89.5° E longitude, covering the southwestern coastal districts of Satkhira, Khulna, and Bagerhat. The Sundarbans Mangrove Forest, located at the confluence of the Ganges, Brahmaputra, and Meghna River systems, forms the largest contiguous tidal halophytic mangrove forest in the world. Spanning approximately 10,000 km² across Bangladesh and India, it plays a crucial role in maintaining the ecological and socio-economic stability of the region. The Bangladeshi portion of the Sundarbans alone covers around 6,017 km² and represents about 60% of the total forest area (Ghosh *et al.,* 2016; Roy *et al.*, 2025).

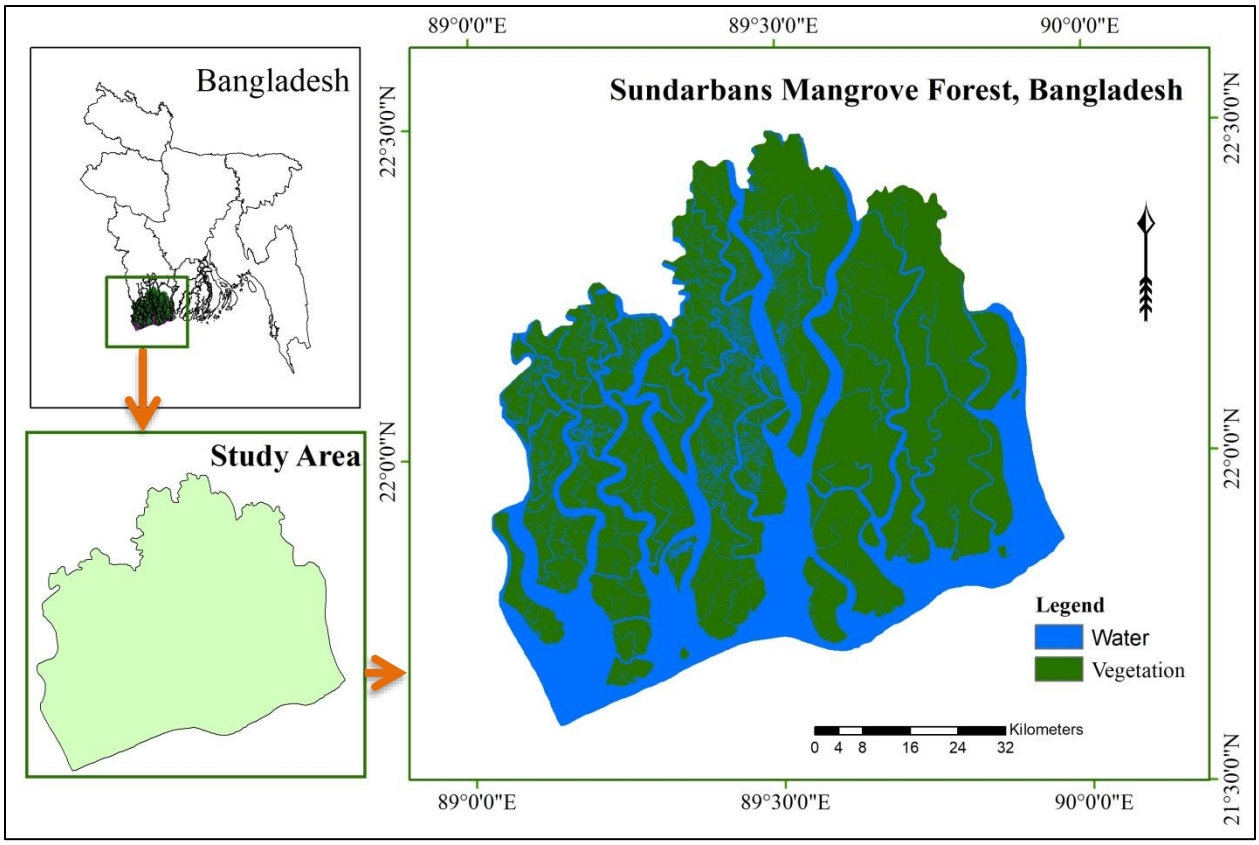

Figure 1: Study Area Map

Climatically, the Sundarbans experience a humid tropical monsoon environment with three distinct seasons: summer (March–May), monsoon (June–September), and winter (October–February). The region receives annual precipitation ranging from 1,500 mm to 2,500 mm and has a mean temperature between 20°C in winter and 34°C in summer (Dasgupta *et al.*, 2015). These climate characteristics influence seasonal water levels and vegetation patterns.

Hydrologically, the forest is shaped by semi-diurnal tides from the Bay of Bengal, resulting in regular inundation and exposure. These tides form estuarine systems, intertidal mudflats, tidal creeks, and brackish water channels, helping the forest buffer storm surges and support sediment and nutrient cycling.

Ecologically, the forest hosts salt-tolerant mangrove species such as *Heritiera fomes* (Sundri), *Excoecaria agallocha* (Gewa), and *Sonneratia apetala* (Keora), which stabilize the shoreline and contribute to ecological services like carbon sequestration and water purification (Patra, 2024; Uddin *et al.*, 2014).

The Sundarbans also shelters globally threatened species such as the Royal Bengal Tiger, estuarine crocodiles, and Irrawaddy dolphins, and supports local livelihoods through fisheries, honey collection, fuelwood, and traditional medicine.

2.2 Remote Sensing Data Acquisition

To comprehensively monitor land cover transformations within the Sundarbans Mangrove Forest over a five-decade period (1975–2025), multi-temporal satellite imagery from the Landsat program was employed. The Landsat program, jointly managed by NASA and the United States Geological Survey (USGS), provides one of the longest continuous records of Earth observation and is considered highly suitable for temporal change analysis due to its moderate spatial resolution, multispectral capabilities, and consistent revisit intervals. All imagery was accessed and downloaded via the USGS Earth Explorer platform, which offers open-access

satellite datasets suitable for long-term environmental monitoring.

For this study, data were retrieved from four different Landsat sensors- Landsat-2 Multispectral Scanner System (MSS), Landsat-5 Thematic Mapper (TM), Landsat-8 Operational Land Imager (OLI), and Landsat-9 OLI-2. The selection of these sensors was based on their availability for the corresponding time periods and their compatibility in terms of spatial and spectral resolutions necessary for land cover classification. Specifically, images were selected for the years 1975, 1988, 1995, 2005, 2015, and 2025 to provide a decadal interval framework, capturing long-term land surface dynamics. The detailed metadata, including sensor type, path/row identifiers under the Worldwide Reference System (WRS), and acquisition dates, are summarized in Table 1.

Table 1. Landsat Imagery Details

Year	**Sensor**	**Path/Row (WRS)**	**Acquisition Date**
1975	Landsat-2 MSS	147/045, 148/044 (WRS-1)	27 & 28 March
1988	Landsat-5 TM	137/045, 138/045 (WRS-2)	19 Feb & 25 Jan
1995	Landsat-5 TM	137/045, 138/045 (WRS-2)	21 & 28 Jan
2005	Landsat-5 TM	137/045, 138/045 (WRS-2)	16 & 07 Jan
2015	Landsat-8 OLI	137/045, 138/045 (WRS-2)	28 Jan & 04 Feb
2025	Landsat-9 OLI	137/045, 138/045 (WRS-2)	15 & 22 Jan

To minimize seasonal bias and ensure spectral consistency, only dry season images (January to March) with less than 10% cloud cover were used (Bhattacharjee *et al.*, 2021). This approach improves reflectance quality by avoiding monsoon-related distortions.

While 1985 would have been ideal for maintaining temporal symmetry, cloud-free imagery for that year was unavailable. Following similar studies (Ghosh *et al.*, 2016; Chowdhury & Hafsa, 2022), 1988 was selected as the closest viable substitute.

Given the extensive spatial footprint of the Sundarbans, particularly under the WRS-1 system used for Landsat MSS data, multiple adjacent scenes were required to achieve full spatial coverage. As a result, scene mosaicking was carried out for the years where a single path/row combination was insufficient-most notably for the 1975 MSS dataset. This ensured that the entire Bangladeshi portion of the Sundarbans was consistently represented across all temporal snapshots, thereby enhancing the reliability of comparative land cover analysis.

A detailed visual representation of the entire methodological framework, including preprocessing, classification, and post-classification analyses, is illustrated in Figure 2. This workflow chart serves as a step-by-step guide to the remote sensing and GIS-based approach employed in this study for land cover change detection in the Sundarbans from 1975 to 2025.

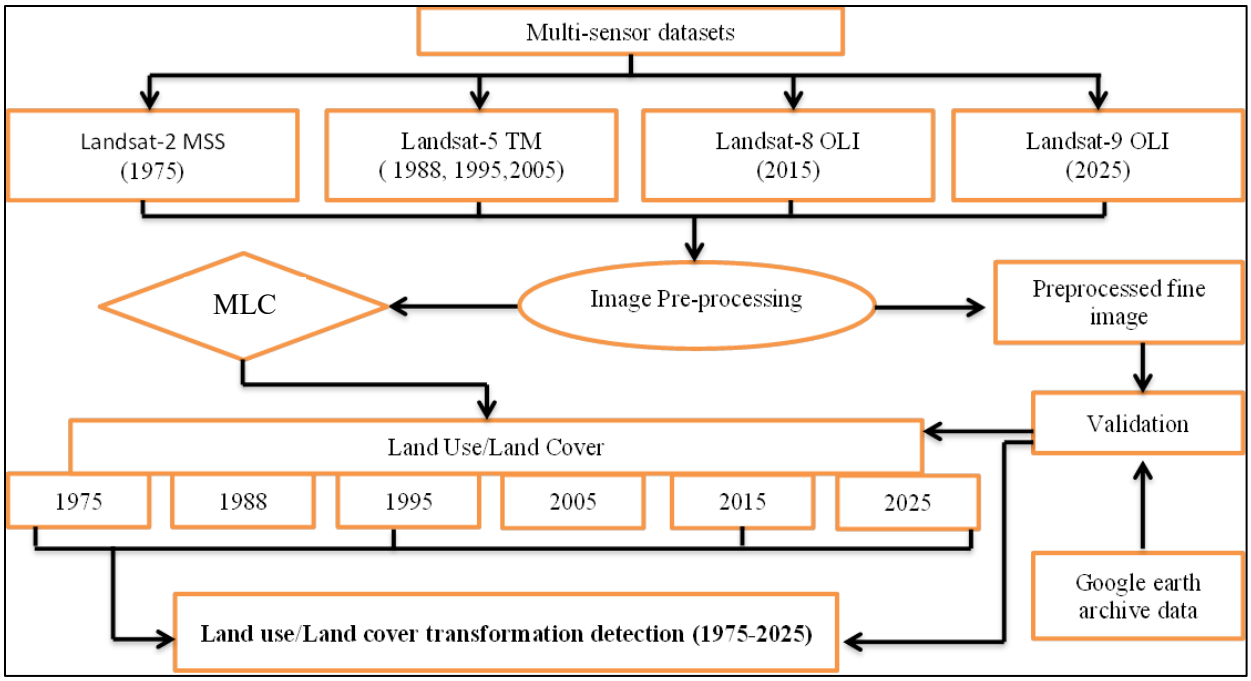

Figure 2: Methodological Workflow of Remote Sensing-Based Land Cover Classification in the Sundarbans (1975–2025).

2.3 Image Preprocessing

Accurate land cover classification in multi-temporal studies heavily depends on comprehensive image preprocessing to ensure consistency and comparability across datasets acquired from different sensors over several decades. Therefore, a systematic preprocessing protocol was adopted to address variations in radiometric response, geometric alignment, sensor-specific artifacts, and temporal differences in data acquisition.

Radiometric and Atmospheric Correction

The Landsat-2 MSS imagery from 1975, lacking Level-2 surface reflectance products, was calibrated by converting Digital Numbers (DNs) to Top-of-Atmosphere (TOA) reflectance using sensor-specific coefficients and solar angle adjustments (Chander et al., 2009; Tucker, 1979). For Landsat-5 TM, Landsat-8 OLI, and Landsat-9 OLI-2, Collection 2 Level-2 surface reflectance products were used. These are atmospherically corrected using the LaSRC algorithm and 6S radiative transfer model, ensuring spectral consistency (Vermote *et al.*, 2016; Roy *et al.*, 2014).

Geometric Correction and Reprojection

To align all images spatially for overlay and analysis, geometric correction and reprojection were performed. All datasets were reprojected to the WGS 1984 UTM Zone 46N coordinate system using ArcGIS 10.8. This step ensured consistent pixel alignment and spatial accuracy, allowing for seamless cross-year comparisons and precise spatial analyses of change patterns (Jensen, 2015).

Destriping and Resampling (MSS Data)

Landsat-2 MSS images exhibited striping artifacts due to sensor limitations. These were mitigated using a Fourier transform-based destriping filter in ENVI 5.3. The original 60-meter resolution was resampled to 30 meters using bilinear interpolation for compatibility with later datasets (Bhattacharjee *et al.,* 2021. This resampling was essential for maintaining consistency across spatial datasets and ensuring compatibility during classification and transformation analysis (Islam & Bhuiyan, 2018).

Image Mosaicking and Layer Stacking

For years requiring multiple scenes (especially MSS data), adjacent path/row images were mosaicked using ENVI 5.3. Bands were then stacked to generate multiband composites, which were clipped to the Sundarbans study area using a predefined boundary shapefile (Patra, 2024).

2.4 Maximum Likelihood Classification (MLC)

To classify the land cover types within the Sundarbans Mangrove Forest across the six reference years (1975, 1988, 1995, 2005, 2015, and 2025), a supervised classification technique known as the Maximum Likelihood Classifier (MLC) was employed. MLC is widely recognized for its effectiveness in classifying complex and heterogeneous landscapes, particularly in mangrove ecosystems where spectral overlap between vegetation classes is common (Lu & Weng, 2007; Ghosh et al., 2016; Kundu et al., 2020; Negassa et al., 2020). Among various available classification algorithms, MLC was chosen for its robustness in pixel-based statistical modeling and its proven suitability in previous multi-temporal land cover studies in similar environments. Compared to object-based or machine learning classifiers like Random Forest or Support Vector Machines, MLC offers a balance between classification accuracy and computational efficiency, especially when high-resolution training samples and consistent spectral bands are available.

The algorithm assumes a normal (Gaussian) distribution of reflectance values for each land cover class and assigns each pixel to the class with the highest probability. Four distinct land cover classes were defined based on ecological relevance and visual interpretability: Water, Bare Soil, Sparse Forest, and Dense Forest. These categories represent both natural and anthropogenically altered landscapes in the Sundarbans. Training samples for each class were carefully selected for all reference years using a combination of field knowledge, visual inspection, and high-resolution Google Earth Pro imagery. Particular attention was given to ensuring temporal consistency in training data to allow for valid comparisons across decades.

The classification procedure was carried out using ArcGIS 10.8, and the raw output was further refined using a 3×3 majority filter. This smoothing technique helps remove isolated misclassified pixels, commonly referred to as "salt-and-pepper noise," thereby improving the spatial coherence of classified patches.

The final classified maps for all six years serve as the foundation for land cover change detection and spatial transformation analysis. These maps are presented in the Results section (Figures 3–5) to demonstrate the temporal dynamics and spatial distribution of each land cover category over the five-decade study period.

Note: The detailed visual outputs of the classification process, including comparative MLC maps for 1975 to 2025, are provided in Section 3 (Results and Discussion).

2.5 Land Cover Transformation Analysis

Land cover change detection was performed using the classified maps through a series of geospatial operations in ArcGIS 10.8. Classified rasters were first converted to vector format, and change zones between consecutive time periods were identified using intersect and dissolve operations. Polygon geometry was then calculated to determine area values (in square kilometers), and the resulting attribute tables were exported to Microsoft Excel for temporal comparison and transition matrix generation.

2.6 Accuracy Assessment

To evaluate the reliability of the classified land cover maps across the six temporal datasets (1975, 1988, 1995, 2005, 2015, and 2025), a rigorous accuracy assessment protocol was followed. A stratified random sampling technique was employed, with approximately 100 reference points generated per year to ensure balanced coverage of all land cover classes.

For the years 1988 to 2025, validation of these points was conducted using high-resolution historical imagery from Google Earth Pro (Bhattacharjee *et al.,* 2021), which allowed precise visual interpretation and cross-verification with classified outputs. In contrast, the 1975 classification lacked access to such high-resolution temporal data; therefore, accuracy validation for this year was based on expert interpretation of the Landsat MSS imagery and corroboration with historical land use maps and ancillary data sources (Foody, 2002).

The following key accuracy metrics were computed:

$$\text{Overall Accuracy (\%)} = \left(\frac{\text{Total Number of Correctly Classified Pixels}}{\text{Total Number of Reference Pixels}}\right) \times 100$$

$$\text{Kappa} = \frac{N\sum xii - \sum xi + x + i}{\text{N}^2 - \sum \text{xi} + \text{x} + \text{i}}$$

Where:

- xii = Number of correctly classified pixels in the ith class (diagonal elements)
- xi= Row totals (classified totals)
- $x + i$ = Column totals (reference totals)
- N = Total number of reference pixels

Across all classification years, the assessment results demonstrated consistently strong accuracy levels. Overall Accuracy (OA) and Kappa Coefficient were calculated for each classification year. OA ranged from 84.0% (1975) to 92.3% (2015), and Kappa values consistently exceeded 0.80, with the highest (0.91) in 2015. The relatively lower accuracy in 1975 reflects limitations of coarser-resolution MSS data. Dense Forest consistently recorded the highest Producer's and User's Accuracy, while Sparse Forest and Bare Soil occasionally showed lower values due to intermediate spectral responses. These findings confirm the robustness of the MLC method in mapping long-term land cover change in the Sundarbans.

3. Results and Discussion

3.1 Results

The supervised Maximum Likelihood Classification (MLC) applied across six distinct periods- 1975, 1988, 1995, 2005, 2015, and 2025 revealed clear and compelling land cover transitions within the Sundarbans Mangrove Forest. Leveraging multi-temporal Landsat datasets and advanced classification techniques, four primary land cover categories were delineated: **Water, Bare Soil, Sparse Forest,** and **Dense Forest**. The classified land cover maps across these years are presented in **Figure 3**, while the quantified land cover areas and their corresponding percentages are summarized in **Table 2.**

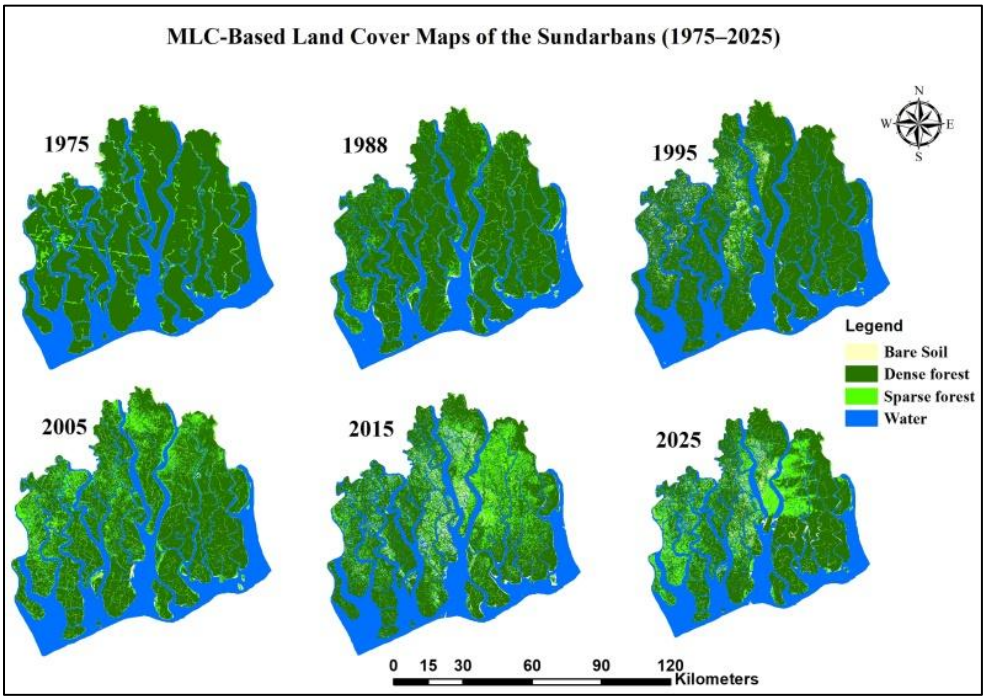

Figure 3: MLC-based Land Cover Maps of the Sundarbans (1975–2025)

A notable and continuous decline in Dense Forest cover was observed over the five-decade span. In 1975, Dense Forest covered approximately 3914.06 km², accounting for 65.17% of the study area. By 2025, this figure had diminished to 2697.82 km² (44.94%), reflecting a net loss of 1216.24 km²-equivalent to a 31.07% reduction. The classified imagery clearly demonstrates a substantial decline in Dense Forest cover, especially in core zones, which corresponds with areas known to be affected by salinity intrusion, reduced freshwater inflow, and increasing anthropogenic pressure such as settlement expansion and resource extraction (Giri *et al.*, 2015; Patra, 2024). Kanjin *et al*. (2024) similarly observed a declining vegetation trend using NDVI analyses, particularly in the southern Sundarbans, reinforcing the degradation patterns presented here. Spatially, this decline was concentrated along the southern and southwestern tidal fronts, where erosion and saline inundation are prevalent.

In contrast, Sparse Forest areas increased markedly, expanding from 254.31 km² (4.23%) in 1975 to 1229.99 km²

(20.49%) in 2025. This 383.67% increase signifies widespread forest thinning, which may reflect not only ecological stressors like cyclonic damage and altered tidal flow but also partial regeneration in previously degraded zones (Dasgupta *et al.,* 2015; Uddin *et al.,* 2014). These transitional areas often represent intermediate stages between dense forest and degraded landscapes and were mostly observed in the central and inland buffer regions.

The area classified as Bare Soil also demonstrated a significant increase, rising from 77.52 km² (1.29%) in 1975 to 309.30 km² (5.15%) in 2025, an approximate 299.06% gain. The observed decrease in Bare Soil area in 2005 is likely due to natural sediment stabilization and subsequent partial revegetation, leading to the reclassification of these areas as Sparse Forest during the classification process. This interpretation is supported by the substantial concurrent increase in Sparse Forest, indicating possible ecological recovery in relatively undisturbed sedimentary zones. This change indicates continued deforestation, land conversion for aquaculture, and exposure of formerly vegetated surfaces due to erosion and salinity-induced dieback (Ghosh *et al.,* 2016; Islam & Bhuiyan, 2018). Bare Soil was frequently identified near human-modified zones and along reclaimed embankments, where vegetation loss is commonly observed.

Interestingly, Water bodies remained relatively stable in total area across the five decades, fluctuating from 1760.14 km² (29.31%) in 1975 to 1766.15 km² (29.42%) in 2025. While the net change (a 0.34% increase) appears marginal, the fluctuation patterns-particularly in 1995 (31.86%) and 2005 (30.65%)-indicate dynamic processes of tidal encroachment, sedimentation, and seasonal water level variation. These fluctuations may also be partially influenced by annual variation in satellite acquisition timing and hydrological regime changes related to upstream flow alterations (Roy *et al.,* 2014; Chander *et al.,* 2009).

Table 2. Land Cover Area Change (1975–2025)

Year	Water (km²)	Area (%)	Bare Soil (km²)	Area (%)	Sparse Forest (km²)	Area (%)	Dense Forest (km²)	Area (%)
1975	1760.14	29.31	77.52	1.29	254.31	4.23	3914.06	65.17
1988	1729.92	28.79	117.26	1.95	295.36	4.92	3865.54	64.34
1995	1912.89	31.86	215.03	3.58	193.49	3.22	3681.84	61.33
2005	1840.07	30.65	147.17	2.45	750.40	12.5	3265.61	54.40
2015	1763.21	29.37	215.58	3.59	1187.38	19.78	2837.11	47.26
2025	1766.15	29.42	309.30	5.15	1229.99	20.49	2697.82	44.94

These transformations collectively illustrate critical ecosystem degradation trends over five decades. The consistent reduction in dense forest, coupled with rising sparse forest and bare soil areas, reflects increasing pressure on the mangrove ecosystem. These patterns echo findings from other regional and global mangrove studies emphasizing the link between anthropogenic activities, climatic stress, and mangrove transformation (Emch & Peterson, 2006; Giri *et al.,* 2015; Sunkur *et al.,* 2024; Roy *et al.,* 2025). The results underscore the urgency of implementing conservation policies, regulating human interventions, and enhancing freshwater flow regimes to protect and restore mangrove habitats.

3.2 Land Cover Transformation Analysis (1975–2025)

The land cover transformation dynamics of the Sundarbans Mangrove Forest over the fifty-year period from 1975 to 2025 provide critical insights into how tidal, sedimentary, and human-driven processes have reshaped one of the world's most ecologically vital deltaic ecosystems. Based on the classified outputs of the supervised Maximum Likelihood Classification (MLC), transitions among four key land cover classes-**Water, Bare Soil, Sparse Forest, and Dense Forest** were assessed. These transitions, visualized in **Figures 4 to 7** and data are summarized in **Table 3**, illustrate both degradation trends and isolated zones of regeneration.

As illustrated in Table 3, transformations from Dense Forest to Sparse Forest alone constituted over 60% of the total changed area, indicating significant canopy degradation and structural fragmentation. Dense Forest also experienced substantial conversions to Bare Soil (10.79%) and Water (6.22%), reinforcing a long-term trend of ecosystem stress. In contrast, positive transitions, such as Sparse Forest to Dense Forest (4.40%) or Bare Soil to vegetation classes (approximately 1%), were relatively minor, highlighting the limited scale of natural regeneration or reforestation. These

trends suggest that degradation processes, including salinity intrusion, erosion, and anthropogenic encroachment, have outpaced recovery efforts during the study period. This broader context sets the stage for a more detailed spatial interpretation in the subsections that follow.

Table 3: Major Land Cover Transitions in the Sundarbans (1975–2025)

Major Transformation		Area in **km²**	**% of the total changed area**
From	To		
Water	Bare soil	77.35	4.41
	Sparse forest	65.51	3.74
	Dense forest	49.49	2.82
Dense forest	Water	109.12	6.22
	Bare soil	189.08	10.79
	Sparse forest	1054.37	60.12
Bare Soil	Water	36.41	2.08
	Sparse forest	9.35	0.53
	Dense forest	9.73	0.55
Sparse forest	Water	52.83	3.01
	Bare soil	23.35	1.33
	Dense forest	77.11	4.40
Total		1753.7	100

Water Body Transformation

Water bodies in the Sundarbans are dynamic, heavily influenced by tidal influx, channel morphology, and seasonal sedimentation. During the study period, a total of 77.35 km² of water bodies were transformed into Bare Soil, primarily due to sediment deposition and lateral accretion processes characteristic of active deltaic regions (Giri *et al.,* 2015). Additionally, 65.51 km² and 49.49 km² of water transitioned into Sparse Forest and Dense Forest, respectively. Figure 4, shows these transitions often occurred along stabilized sediment bars, tidal flats, and near river mouths (Kundu *et al.,* 2020; Bhattacharjee *et al.,* 2021), where mangroves naturally colonize newly formed land. These findings align with Kanjin et al. (2024), who also identified sediment accretion zones as potential regeneration sites for mangroves in degraded estuarine margins. This ecological succession reflects the inherent adaptive capacity of mangrove vegetation in re-establishing on fresh alluvium process well documented in deltaic estuarine systems (Kuenzer *et al.,* 2011; Sunkur *et al.,* 2024). However, the spatial extent of such positive transitions was relatively minor compared to the overall transformation matrix, indicating limited net gain in vegetation from water bodies.

Figure 4: Transformation of Water Body

Figure 5: Transformation of Bare Soil

Bare Soil Transformation

The Bare Soil class exhibited both regressive and progressive transformations. Notably, 36.41 km² of bare land areas reverted to Water, indicative of submergence due to tidal encroachment, channel expansion, or erosion of unstable sediment deposits. Conversely, 9.35 km² and 9.73 km² transitioned into Sparse and Dense Forest, respectively-evidence of active mangrove regeneration. These changes may be attributed to sediment stability, natural revegetation processes, or targeted afforestation efforts within conservation projects (Negassa *et al.,* 2020). As shown in Figure 5, these gains are often observed in the interior zones where sediment retention is high and anthropogenic pressure is relatively low. Such patterns underscore the role of geomorphological suitability and tidal sediment balance in supporting vegetation recovery (Roy *et al.,* 2014; Ghosh *et al.,* 2016). Moreover, affirm the resilience of mangrove species when favorable

hydrological and salinity conditions are restored (Joshi *et al.,* 2016).

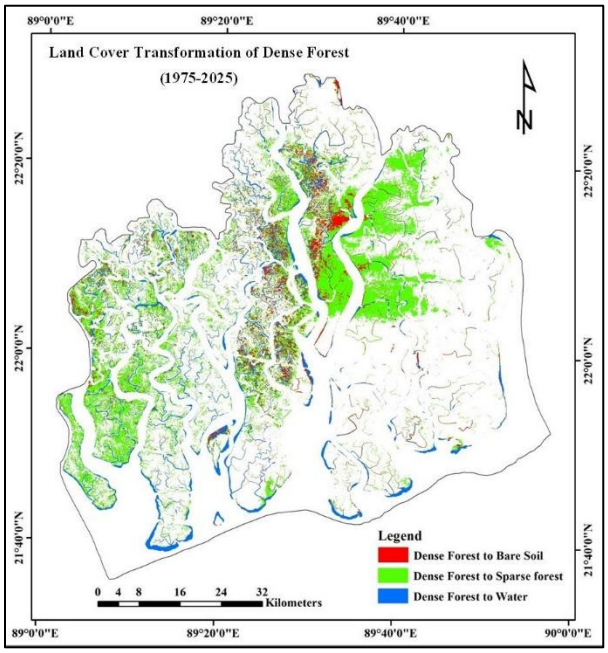

Figure 6: Transformation of Dense Forest

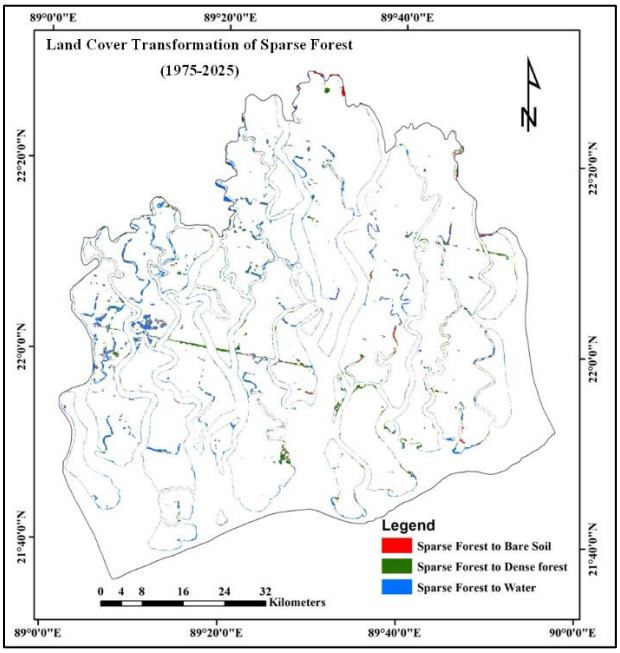

Figure 7: Transformation of Sparse Forest

Dense Forest Transformation

Among all categories, Dense Forest exhibited the most alarming rates of transformation. Approximately 109.12 km² of dense forest was lost to Water, reflecting the growing influence of estuarine erosion, relative sea-level rise, and tidal scouring, particularly along major distributaries and the southern coastal margins (Dasgupta *et al.,* 2015; Bomer *et al.,* 2020). An additional 189.08 km² was converted to Bare Soil, a likely consequence of deforestation for aquaculture expansion, infrastructural encroachment, or clear-cutting, often exacerbated by salinity intrusion and soil degradation (Islam & Bhuiyan, 2018). The most extensive transformation, however, involved 1054.37 km² of dense Forest converting into Sparse Forest, indicating progressive thinning of canopy structure, fragmentation of tree stands, and overall ecological decline. This conversion often occurs in salinity-prone zones and along forest edges, suggesting declining forest health due to prolonged exposure to stressors (Patra, 2024; Uddin *et al.,* 2014). Figure 6 illustrates these spatial transformations concentrated around areas of high anthropogenic interaction, including embankment breaches and shrimp culture zones.

Sparse Forest Transformation

The Sparse Forest class reflects a transitional state-both vulnerable to degradation and capable of recovery under favorable conditions. A total of 52.83 km² of Sparse Forest reverted to Water, which may be associated with tidal intrusion, erosion along forest edges, and breaching of embankments, particularly in low-elevation, cyclone-exposed areas (Potapov *et al.,* 2012). On a more positive note, 77.11 km² of Sparse Forest transitioned into Dense Forest, demonstrating the potential for structural regeneration when ecological stress is mitigated. However, 23.35 km² of Sparse Forest transitioned into Bare Soil, signifying continued degradation, potentially due to salt stress-induced dieback or small-scale human clearings. As seen in Figure 7, these transitions are spatially dispersed, with regeneration mostly occurring in the northern and central forest regions, while degradation hotspots align with human proximity and reduced freshwater inflow (Giri *et al.,* 2011; Chander *et al.,* 2009).

Collectively, these spatial transitions underscore the ecological vulnerability of the Sundarbans. Dense Forest retreat and Sparse Forest expansion reflect long-term structural degradation and landscape fragmentation. The transformation maps (Figures 3–6) identify spatial hotspots-particularly along tidal creeks, deltaic edges, and human-influenced zones-where intervention is urgently needed.

These findings align with global assessments of mangrove loss and emphasize the importance of sediment dynamics, hydrological regime shifts, and anthropogenic drivers (Roy *et al.,* 2014; Vermote *et al.,* 2016). Mapping such transformations provides empirical insight to guide ecosystem restoration, zonal conservation, and climate adaptation strategies tailored to this globally significant mangrove forest.

3.3 Spatial Dynamics of Land Cover Gains and Losses (1975–2025)

To complement the transformation analysis presented earlier, this section quantitatively explores the spatial dynamics of land cover gains and losses across four major land cover classes-Water, Bare Soil, Sparse Forest, and Dense Forest-between 1975 and 2025 in the Bangladeshi Sundarbans. This analysis provides additional insight into the net structural changes and ecological balance shifts over the five-decade period. The comparative figures and metrics in Figure 6, 7 and 8 reflect the relative resilience and vulnerability of each land cover class.

Dense Forest exhibited the most pronounced loss, accounting for a staggering 1352.57 km² or 77.13% of the total transformed area. This decline is consistent with prior spatial assessments and highlights intense anthropogenic deforestation, hydrological stress, and salinity intrusion, especially in southern and peripheral zones. Despite this considerable loss, only 136.33 km² (7.77%) of Dense Forest was gained, indicating poor rates of regeneration and canopy closure over time.

In contrast, Sparse Forest demonstrated a net increase in extent. It gained approximately 1129.23 km² (64.39%)-the largest among all classes-while losing only 153.29 km² (8.74%). This pattern signifies a widespread transformation from Dense to Sparse Forest, indicative of forest thinning and structural degradation. However, it also highlights some ecological resilience, where previously degraded zones retained partial vegetation cover.

Bare Soil gained 289.78 km² (16.52%), often from cleared forest zones and receding waters, while it lost only 55.49 km² (3.16%) to re-vegetation or inundation. The net increase in Bare Soil areas points to grow land degradation and exposure of previously vegetated surfaces, especially along inland and estuarine fringes.

Water bodies displayed relative balance, with a gain of 198.36 km² (11.31%) and a nearly equivalent loss of 192.35 km² (10.97%). These changes align with tidal dynamics, sedimentation, and seasonal riverbank shifts. The marginal net gain in water area affirms the tidal estuary's hydro-geomorphic volatility.

This land cover gain-loss matrix, serves as a vital spatial diagnostic tool to understand land degradation patterns and recovery potentials. The corresponding Figure 8 provides a visual comparison, emphasizing the disproportionate losses in Dense Forest and the significant rise in Sparse Forest and Bare Soil.

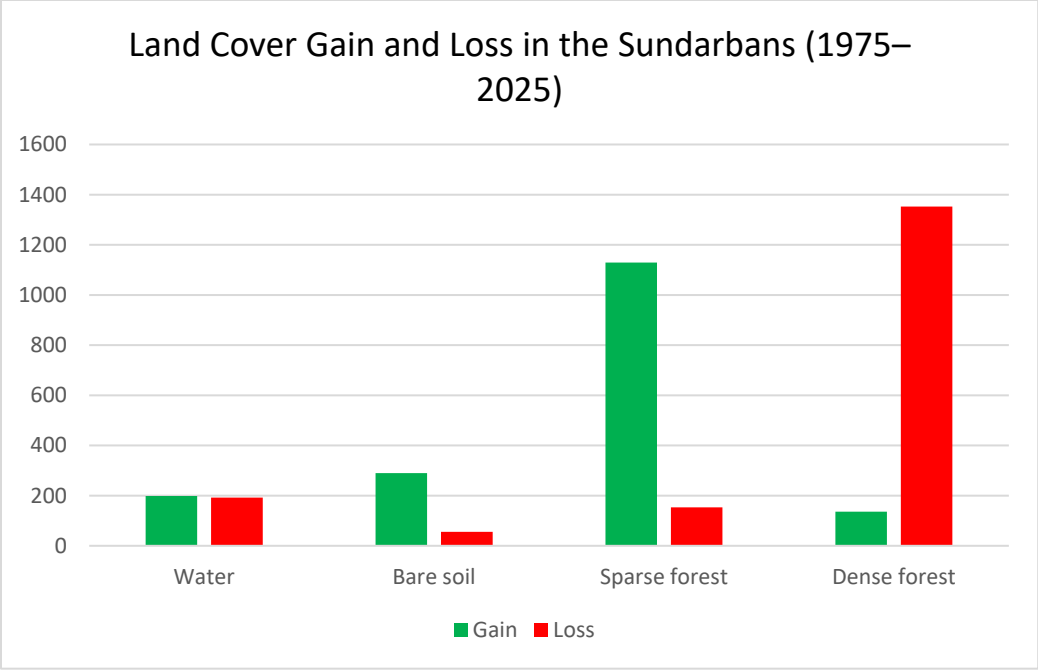

Figure 8. Comparative Gain and Loss of Land Cover Classes in the Bangladeshi Sundarbans (1975–2025)

These results collectively reflect the asymmetric patterns of degradation and regeneration, offering a foundational dataset for ecosystem management strategies and prioritization of restoration zones.

3.4 Discussion

The results of the last five-decade analysis reveal significant transformations in the land cover of the Sundarbans Mangrove Forest, underscoring the intensifying ecological vulnerability of this critical coastal ecosystem. The most striking finding is the extensive degradation of Dense Forest cover, which declined by approximately 1216.24 km² (31.07%) between 1975 and 2025. This loss corresponds to the largest proportion of total land cover transformation, where more than 1352.57 km² of Dense Forest was converted-largely into Sparse Forest (1054.37 km²), and to a lesser extent into Bare Soil (189.08 km²) and Water (109.12 km²). These transitions point directly to extensive deforestation, canopy thinning, and habitat fragmentation, largely driven by escalating anthropogenic activities including unregulated aquaculture, illegal logging, embankment breaches, and saltwater intrusion (Giri et al., 2015; Islam & Bhuiyan, 2018).

The expansion of Sparse Forest, by more than 975 km² over the study period, represents a mixed ecological signal. While the net increase suggests partial vegetation persistence and regeneration in certain zones, particularly where afforestation and sediment stabilization occurred, the dominance of Dense-to-Sparse Forest transitions (over 60% of total transformations) highlights structural degradation and the weakening of mangrove ecosystem integrity. This trend reflects environmental stress due to hydrological alteration, salinity fluctuation, and storm impacts (Uddin et al., 2014; Sunkur et al., 2024). Consistent with this interpretation, Kanjin et al. (2024) found that frequent cyclone events and poor soil moisture in recent years were key contributors to declining mangrove health in large tracts of the Sundarbans.

Similarly, the 299.06% increase in Bare Soil-expanding from 77.52 km² in 1975 to 309.30 km² in 2025-signals growing land degradation and failed reforestation in sediment-exposed and anthropogenically altered zones. These regions, often adjacent to reclaimed areas and aquaculture plots, show signs of prolonged salinization and erosion, especially where vegetation fails to re-establish (Ghosh et al., 2016; Roy et al., 2014). On the positive side, limited gains from Bare Soil to vegetated categories (Sparse and Dense Forest) suggest ecological resilience in selected micro-environments where tidal flow and sediment supply remain intact.

Water bodies exhibited relatively minor net change (a gain of just 6 km² over five decades), despite dynamic local-scale transitions. Approximately 192.35 km² of water area was lost to terrestrial categories, mainly Bare Soil and vegetation, while 198.36 km² was gained. These transitions reflect the fluid hydromorphology of the Sundarbans, shaped by tidal inflow, sediment accretion, riverbank migration, and possibly upstream water management interventions such as the Farakka Barrage (Roy et al., 2014; Patra, 2024). Although the areal extent appears stable, this study's scope did not include bathymetric change, which remains a critical knowledge gap for assessing tidal basin health and future flood resilience. Recent research, however, has shown that mangrove landscapes in the Sundarbans are actively adjusting their surface elevation through sediment accretion, helping them adapt to human-altered tidal regimes and local sea-level rise (Bomer et al., 2020).

Spatial analysis reveals clear patterns of degradation and regeneration. Dense Forest loss was prominent near southern tidal interfaces and river mouths, while Sparse Forest gains were concentrated in central and northern buffer zones. Figures 3–6 and the gain-loss matrix in Figure 6, 7 and 8 affirm these trends. Notably, gains in Sparse Forest (1129.23 km²) significantly outpaced its losses (153.29 km²), underscoring a widespread shift toward a lower-structure forest condition, which, although ecologically weaker, still offers critical services like erosion control and carbon storage.

From a methodological standpoint, the use of Maximum Likelihood Classification (MLC) proved effective in capturing complex transitions across time and space. A similar approach was adopted by Chowdhury and Hafsa (2022), who applied supervised MLC on multi-temporal Landsat data to assess long-term land cover dynamics in the Bangladeshi Sundarbans with high classification accuracy and robust transition analysis. MLC allowed categorical differentiation that was both statistically robust and ecologically meaningful, outperforming index-based classification approaches such as NDVI for multitemporal landscape mapping in mangrove ecosystems (Kanjin et al., 2024; Ghosh et al., 2016; Lu & Weng, 2007).

Management implications of these findings are substantial. The Sundarbans resilience depends on implementing integrated land-use strategies that combine remote sensing monitoring with ground-based afforestation, salinity management, and freshwater regime restoration. High-risk transformation zones identified in this study, especially southern fringes and dense-to-sparse forest corridors-should be prioritized for conservation investment. In addition, promoting community-managed buffer zones and sustainable aquaculture practices can mitigate anthropogenic pressure and enhance long-term ecosystem stability (Uddin et al., 2014; Patra, 2024).

In summary, this study observed extensive forest degradation, limited regeneration, and shifting ecological baselines in the observed Sundarbans Mangrove Forest from 1975 to 2025. The spatial and categorical trends presented here serve as a foundation for evidence-based policy and restoration initiatives aimed at protecting this globally critical and climatically vulnerable landscape.

4. Conclusion

This study presents a comprehensive, five-decade assessment of land cover dynamics in the Bangladeshi Sundarbans Mangrove Forest, utilizing supervised Maximum Likelihood Classification (MLC) on atmospherically corrected Landsat imagery. By classifying and analyzing changes in four ecologically significant land cover types-Water, Bare Soil, Sparse Forest, and Dense Forest-this research reveals long-term structural degradation and ecological stress across the mangrove ecosystem. Transformation matrices and spatial gain-loss assessments indicate that Dense Forest areas have undergone substantial loss, largely due to salinity intrusion, reduced freshwater flow, and anthropogenic pressures. While increases in Sparse Forest and Bare Soil suggest widespread vegetation thinning and land exposure, these transitions reflect degradation rather than true ecological recovery. The apparent stability in surface water extent masks deeper hydrological transformations, underscoring the need for integrated studies on water depth, sedimentation, and quality.

This study contributes novel insight by combining multi-decadal categorical classification with spatial transition mapping, offering high-resolution evidence for long-term ecosystem vulnerability. To ensure sustainability, ecosystem-based management strategies-such as afforestation, salinity monitoring, freshwater regime restoration, and land-use regulation-should be prioritized in ecologically sensitive transition zones. Moving forward, future studies should consider integrating bathymetric data, seasonal spectral indices, and climate model projections to enhance understanding of tidal dynamics and resilience pathways. Overall, this research provides a strong foundation for policy planning, restoration prioritization, and adaptive conservation of one of the world's most vulnerable coastal landscapes.

Conflict of the interest: The authors declare no conflicts of interest related to the publication of this article.

References:

Al-doski, J., Mansor, S. B. and Shafri, H. Z. M. 2013. Image classification in remote sensing. International Journal of Engineering Research and Technology (IJERT), 2(11), 2278–0181.

Bhattacharjee, S., Islam, M. T., Kabir, M. E. and Kabir, M. M. 2021. Land-use and land-cover change detection in a north-eastern wetland ecosystem of Bangladesh using remote sensing and GIS techniques. Earth Systems and Environment, 5(2), 319–340. https://doi.org/10.1007/s41748-021-00228-3

Bomer, E. J., Wilson, C. A., Hale, R. P., Hossain, A. N. M. M. and Rahman, F. M. A. 2020. Surface elevation and sedimentation dynamics in the Ganges-Brahmaputra tidal delta plain, Bangladesh: Evidence for mangrove adaptation to human-induced tidal amplification. Catena, 187, 104312. https://doi.org/10.1016/j.catena.2019.104312

Chander, G., Markham, B. L., and Helder, D. L. 2009. Summary of current radiometric calibration coefficients for Landsat MSS, TM, ETM+, and EO-1 ALI sensors. Remote Sensing of Environment, 113(5), 893–903. https://doi.org/10.1016/j.rse.2009.01.007

Chowdhury, M. S. and Hafsa, B. 2022. Multi-decadal land cover change analysis over Sundarbans Mangrove Forest of Bangladesh: A GIS and remote sensing based approach. Global Ecology and Conservation, 37, e02151. https://doi.org/10.1016/j.gecco.2022.e02151

Dasgupta, S., Sobhan, M. I. and Wheeler, D. 2015. Climate change and soil salinity: The case of coastal Bangladesh. Ambio, 44(8), 815–826. https://doi.org/10.1007/s13280-015-0681-5

Emch, M. and Peterson, M. 2006. Mangrove forest cover change in the Bangladesh Sundarbans from 1989–2000: A remote sensing approach. Geocarto International, 21(1), 5–12. https://doi.org/10.1080/10106040608542368

Foody, G. M. 2002. Status of land cover classification accuracy assessment. Remote Sensing of Environment, 80(1), 185–201. https://doi.org/10.1016/S0034-4257(01)00295-4

Ghosh, M. K., Kumar, L. and Roy, C. 2016. Mapping long-term changes in mangrove species composition and

distribution in the Sundarbans. Forests, 7(12), 305. https://doi.org/10.3390/f7120305

Giri, C., Long, J., Abbas, S., Murali, R. M., Qamer, F. M., Pengra, B., and Thau, D. 2015. Distribution and dynamics of mangrove forests of South Asia. Journal of Environmental Management, 148, 101–111. https://doi.org/10.1016/j.jenvman.2014.06.020

Giri, C., Ochieng, E., Tieszen, L. L., Zhu, Z., Singh, A., Loveland, T., ... and Duke, N. 2011. Status and distribution of mangrove forests of the world using earth observation satellite data. Global Ecology and Biogeography, 20(1), 154–159. https://doi.org/10.1111/j.1466-8238.2010.00584.x

Huete, A., Didan, K., Miura, T., Rodriguez, E. P., Gao, X. and Ferreira, L. G. 2002. Overview of the radiometric and biophysical performance of the MODIS vegetation indices. Remote Sensing of Environment, 83(1–2), 195–213. https://doi.org/10.1016/S0034-4257(02)00096-2

Islam, M. M. and Bhuiyan, M. A. H. 2018. A study on remote sensing-based land use classification in the Sundarbans using Landsat imagery. Journal of Environmental Science and Natural Resources, 11(1–2), 113–121.

Jensen, J. R. 2015. Introductory digital image processing: A remote sensing perspective (4th ed.). Pearson Education.

Joshi, N., Baumann, M., Ehammer, A., Fensholt, R., Grogan, K., Hostert, P., ... and Rabe, A. 2016. A review of the application of optical and radar remote sensing data fusion to land use mapping and monitoring. Remote Sensing, 8(1), 70. https://doi.org/10.3390/rs8010070

Kanjin, K. and Alam, B. M. 2024. Assessing changes in land cover, NDVI, and LST in the Sundarbans mangrove forest in Bangladesh and India: A GIS and remote sensing approach. Remote Sensing Applications: Society and Environment, 36, 101289. https://doi.org/10.1016/j.rsase.2024.101289

Kuenzer, C., Bluemel, A., Gebhardt, S., Quoc, T. V. and Dech, S. 2011. Remote sensing of mangrove ecosystems: A review. Remote Sensing, 3(5), 878–928. https://doi.org/10.3390/rs3050878

Kundu, K., Halder, P. and Mandal, J. K. 2020. Forest cover change analysis in Sundarban delta using remote sensing data and GIS. In J. K. Mandal & D. Sinha (Eds.), Intelligent computing paradigm: Recent trends (pp. 85–101). Springer. https://doi.org/10.1007/978-981-13-7334-3_7

Lu, D., and Weng, Q. 2007. A survey of image classification methods and techniques for improving classification performance. Remote Sensing of Environment, 110(3), 337–349. https://doi.org/10.1016/j.rse.2007.03.001

Negassa, M. D., Mallie, D. T., and Gemeda, D. O. 2020. Forest cover change detection using Geographic Information Systems and remote sensing techniques: A spatio-temporal study on Komto Protected forest priority area, East Wollega Zone, Ethiopia. Environmental Systems Research, 9(1), Article 1. https://doi.org/10.1186/s40068-020-0163-z

Patra, T. 2024. Impacts of climate change on the Sundarbans mangrove ecosystem: A comprehensive analysis. International Research Journal of Modernization in Engineering, Technology and Science, 6(8), 1171–1178. https://doi.org/10.56726/IRJMETS60970

Potapov, P. V., Turubanova, S. A., Hansen, M. C., Adusei, B., Broich, M., Altstatt, A., ... and Egorov, A. 2012. Quantifying forest cover loss in Democratic Republic of the Congo, 2000–2010, with Landsat ETM+ data. Remote Sensing of Environment, 122, 106–116. https://doi.org/10.1016/j.rse.2011.08.027

Roy, D. P., Wulder, M. A., Loveland, T. R., Woodcock, C. E., Allen, R. G., Anderson, M. C., ... and Zhu, Z. 2014. Landsat-8: Science and product vision for terrestrial global change research. Remote Sensing of Environment, 145, 154–172. https://doi.org/10.1016/j.rse.2014.02.001

Roy, S. K., Alam, M. S. and Hossain, M. I. 2025. Vegetation dynamics in the Sundarbans Mangrove Forest (1975–2025) using NDVI-based remote sensing analysis. Global Ecology and Conservation, 58, e03493. https://doi.org/10.1016/j.gecco.2025.e03493

Sunkur, R., Hazra, S., Chatterjee, K., and Maiti, R. 2024. Mangrove mapping and monitoring using remote sensing techniques towards climate change resilience. Scientific

Reports, 14, 6949. https://doi.org/10.1038/s41598-024-57563-4

Tucker, C. J. 1979. Red and photographic infrared linear combinations for monitoring vegetation. Remote Sensing of Environment, 8, 127–150. https://doi.org/10.1016/0034-4257(79)90013-0

Uddin, M. S., Shah, M. A. R., Khanom, S. and Nesha, M. K. 2014. Climate change impacts on the Sundarbans mangrove ecosystem services and dependent livelihoods in Bangladesh. Asian Journal of Conservation Biology, 2(2), 152–156.

Vermote, E. F., Justice, C., Claverie, M. and Franch, B. 2016. Preliminary analysis of the performance of the Landsat 8/OLI land surface reflectance product. Remote Sensing of Environment, 185, 46–56. https://doi.org/10.1016/j.rse.2016.04.008